

Age-related myelin degradation burdens microglia clearance function during aging

Shima Safaiyan¹, Nirmal Kannaiyan⁷, Nicolas Snaidero^{1,2}, Simone Brioschi⁸, Knut Biber^{8,9}, Simon Yona⁵, Aimee L. Edinger⁶, Steffen Jung⁵, Moritz J. Rossner^{1,7}, Mikael Simons^{1-4*}

¹Max Planck Institute of Experimental Medicine, Göttingen, Germany

²Institute of Neuronal Cell Biology, Technical University Munich, Munich, Germany

³German Center for Neurodegenerative Diseases (DZNE), Munich, Germany

⁴Munich Cluster of Systems Neurology (SyNergy), Munich, Germany

⁵Department of Immunology, The Weizmann Institute of Science, Rehovot, Israel.

⁶Department of Developmental and Cell Biology; University of California, Irvine; USA

⁷Department of Psychiatry, Ludwig-Maximillan University, Munich, Germany

⁸Department of Psychiatry and Psychotherapy, Freiburg, Germany

⁹Department of Neuroscience, University of Groningen, University Medical Center Groningen, The Netherlands

*Correspondence to: M. Simons (Email: msimons@gwdg.de)

Myelin is synthesized as a multilamellar membrane, but the mechanisms of membrane turnover are unknown. We find that myelin pieces are gradually released from aging myelin sheaths and are subsequently cleared by microglia. Myelin fragmentation increases with age and leads to the formation of insoluble, lipofuscin-like lysosomal inclusions in microglia. Thus, age-related myelin fragmentation is substantial leading to lysosomal storage and contributing to microglia senescence and immune dysfunction in aging.

Myelin is formed by oligodendrocytes as a multilamellar structure that encloses segments of axons in the central nervous systems (CNS) of vertebrates ¹. Once myelin is laid down, it is unknown to what extent the sheaths require maintenance and remodeling. Membrane turnover may pose a problem for oligodendrocytes that form up to 80 different myelin sheaths of tightly stacked membrane, but harbour little cytoplasm and few lysosomes, the organelles responsible for membrane degradation. Myelin membrane components are metabolically relatively stable with half-lives on the order of several weeks to months ^{2,3}. Nevertheless, protein/lipid turnover is, in general, necessary to replace potentially impaired molecules with new functional copies in order to combat functional decline ⁴⁻⁷. How do molecules trapped within the numerous layers of tightly compacted membrane enter the degradative system? We tested the hypothesis that myelin degradation occurs in part via shedding of myelin fragments into the extracellular space.

We analyzed the white matter of aging mice (up to 24 months) by electron microscopy to search for myelin breakdown products. We detected multilamellar myelin fragments more frequently in the brain of the older mice, of which some were associated with myelin sheaths, while others were in the extracellular space or inside of cells (**Supplementary Fig. 1**). As fixation artefacts frequently affect the appearance of myelin in chemically fixed tissue, we used high-pressure freezing to fix tissue and confirmed the progressive accumulation of multilamellar myelin fragments with age (**Fig. 1a,b**).

Since some of these myelin fragments were found inside cells, we performed immunohistochemistry to determine whether microglia, the brain phagocytes ⁸⁻¹⁰, were responsible for the uptake of myelin fragments. An increasing number of myelin basic protein (MBP) and proteolipid protein (PLP) immunoreactive puncta co-localized with Iba1-positive microglia with age (**Fig. 1c, Supplementary Fig. 1**). Three-dimensional reconstructions demonstrated that immunoreactive puncta were present inside of microglia (**Fig. 1c**). Since our results suggested that microglia clear away the myelin fragments that accumulate in the

aging brain, we compared microglia number and appearance in young and old animals. Not only had the number of microglia increased in the white matter of old animals as reported previously^{11,12}, but also microglia in contact with myelin (**Supplementary Fig. 2**). Next, the morphology of lysosomes was evaluated to determine whether microglia were actively engaged in membrane degradation. We observed a marked increase in the size of CD68-positive lysosomes in microglia with age. This increase was more pronounced in the white matter than in the grey matter (**Fig. 1d,e**). Similar results were obtained by staining with Lamp1, a marker for late endosomes/lysosomes (**Supplementary Fig. 2**). Since Galectin-3/Mac-2 is known to be involved in myelin phagocytosis¹³, we compared Mac-2 immunostaining in young and old mice and found that the amount of Mac-2 increased in the white matter with age (**Supplementary Fig. 2**). By FACS analysis macrophage infiltration into the aging brain was excluded (**Supplementary Fig. 3**).

Next, we purified microglia from one year old mice to determine the amount of MBP associated with microglia. Notably, western blot analysis of microglial lysates showed that a large fraction of MBP was of high-molecular weight indicating that it forms detergent-insoluble aggregates in microglia (**Fig. 1f**). To validate these findings, we prepared Sarkosyl-insoluble membrane fractions of microglia lysates. High-molecular weight species of MBP also existed in the Sarkosyl-insoluble membrane fraction (**Fig. 1f**). When Sarkosyl extractions were performed on purified myelin, virtually the entire fraction of MBP was solubilized, demonstrating that only the aggregated state of MBP is Sarkosyl-insoluble (**Fig. 1f**).

One of the most specific biomarkers for the age of post-mitotic cells is the accumulation of Sarkosyl-insoluble lipofuscin granules in lysosomes^{14,15}. We confirmed the steady increase in number and volume of lipofuscin granules in microglia with age (**Supplementary Fig. 4**). When comparing the size of lipofuscin inclusions in microglia in the grey and white matter of aged mice, we found that lipofuscin granules were significantly larger in the white matter (**Supplementary Fig. 4**). When microglia were co-stained with MBP or FluoroMyelin, we observed that myelin fragments were frequently associated with lipofuscin suggesting that some of the lipofuscin may arise from myelin membrane remnants (**Fig. 1g**). To determine whether myelin debris uptake results in lipofuscin generation in microglia, we added purified myelin to organotypic hippocampal slice cultures. Already three days after myelin uptake lipofuscin was detected in ~15% of the microglia, where it partially colocalized with internalized myelin (**Supplementary Fig. 5**).

The generation of lipofuscin from myelin was confirmed in *shiverer* mice that form myelin sheaths with only few wraps that are rapidly broken down. We found a significant increase in

lipofuscin in *shiverer* mice as young as P25 demonstrating that myelin degeneration promotes premature lipofuscin formation (**Supplementary Fig. 5**).

These results not only show that microglia actively clear away myelin, but also indicate that this process is associated with the accumulation of undegradable lysosomal aggregates in microglia of the aging brain.

Given that microglia appear to be involved in myelin clearance, we reasoned that blocking lysosomal degradation should lead to the accumulation of myelin fragments in younger mice. Thus, we generated conditional Rab7 KO mice using CX₃CR1^{CreER} animals to specifically interfere with lysosomal function in microglia/macrophage^{16,17}. Cell-specific recombination was confirmed by crossing mice with TdTomato reporter line, which showed TdTomato expression in more than 90% of the microglia (**Supplementary Fig. 6**). In addition, RT-PCR analysis of isolated microglia from control and CX₃CR1^{CreER}:Rab7^{flox/flox} (Rab7^{ΔMG}) mice showed that the Rab7 transcripts were barely detectable in purified Rab7^{ΔMG} microglia (**Supplementary Fig. 6**). Consistent with late endosomal/lysosomal dysfunction, we detected enlarged Lamp1-positive structures in at least 50% of the microglia of Rab7^{ΔMG} mice (**Supplementary Fig. 6**).

Notably, Rab7^{ΔMG} mice developed MBP immunoreactive puncta in microglial earlier (9 month versus 18 months of age in control) and with greater frequency than control mice (**Fig. 2a**). There was a massive accumulation of lipofuscin within microglia in Rab7^{ΔMG} mice and, compared to control mice, lipofuscin was more frequently associated with FluoroMyelin-positive myelin fragments (**Fig. 2b**). Remarkably, the lysosomal inclusions were reminiscent of those observed in microglia in the aging brain of wild-type mice. These data show that blocking lysosomal function in microglia results in intracellular myelin accumulation and in the formation of lysosomal inclusions akin to aging pigment. Additional hallmarks of microglia senescence are shortened and fragmented processes, low-grade activation (as determined by increased MHC-II expression) and a decrease in phagocytic/macropinocytic function¹⁴. Strikingly, microglia in Rab7^{ΔMG} mice possessed shorter processes and exhibited premature upregulation of major histocompatibility complex II (MHC-II) (**Fig. 2d**), and showed a reduced capacity to take up stereotactically injected FITC-Dextran (**Supplementary Fig. 7**). Consistent with a decline in microglia uptake function, we detected multilamellar myelin fragments at increased frequency in microglia of Rab7^{ΔMG} mice (**Supplementary Fig. 7**). To corroborate the age-associated changes of microglia in Rab7^{ΔMG} mice, we acutely isolated microglia from wild-type and of Rab7^{ΔMG} animals and performed RNA-Seq analysis. 550 genes (~3.5% of total) were enriched in microglia of Rab7^{ΔMG} as compared to microglia

from wild-type mice (with an at least 2 fold enrichment; $p < 0.05$; **Supplementary Table 1**). Pathway analysis showed that genes involved in immune function were among the most differentially expressed (**Fig. 2e**). Next, we compared the transcriptional profile of microglia from Rab7^{ΔMG} mice with the profile of microglia from aged mice^{18,19}. 653 genes were upregulated in microglia from aged (24 months) as compared to young (10 weeks) mice (**Supplementary Table 1**). When comparing these two analyses, a striking overlap (133 genes) between upregulated genes, with an overrepresentation of pathway related to immune function (corr. $p < 10^{-9}$), was seen (**Fig. 2f**; **Supplementary Fig. 8**). Overall, these results suggest that dysfunction of the lysosomal pathway induces a phenotype associated with aging in microglia.

We hypothesized that increasing myelin breakdown in mice could exceed the degradative capacity of microglia earlier. Hence, we analyzed whether a single demyelinating event would be sufficient to induce accumulation of aging pigment in microglia. Feeding mice with cuprizone for 4 weeks causes widespread demyelination that is followed by remyelination. We analyzed mice up to 37 weeks after the demyelinating event and quantified lipofuscin volume in microglia in cuprizone-fed and control mice. Lipofuscin increased as early as 9 weeks after cuprizone feeding and continued to increase throughout the experiment (**Fig. 3a**). Myelin fragments were frequently associated with lipofuscin granules even 37 weeks after cuprizone treatment (**Fig. 3c**). MHC-II was, as expected, strongly up-regulated 9 weeks after cuprizone feeding indicating microglial activation. More interestingly, MHC-II expression returned to control levels at week 15 and 23, but was re-expressed 37 weeks after cuprizone feeding (**Fig. 3d**). Thus, age-associated low grade inflammation occurs earlier, when the brain has undergone one event of widespread demyelination.

Next, we analyzed microglia in a mouse model for Pelizaeus-Merzbacher disease with extra copies of the wild-type Plp1 gene (PMD mice)²⁰. These mice develop relatively normal myelin, but long-term stability of myelin is comprised and a large number of the myelin sheaths are gradually broken-down and lost²⁰. We confirmed the progressive demyelinating phenotype, which went along with an increased number of microglia and an upregulation of Mac-2 and MHC-II (**Supplementary Fig. 9**). Myelin fragments were frequently found within microglia (**Fig. 3e**). Importantly, lipofuscin volume in microglia increased more rapidly in the white matter of PMD as compare to wild-type mice (**Fig. 3f**). These changes were accompanied by a decline in macropinocytic function of microglia as shown by FITC-Dextran uptake experiments *in vivo* and amyloid- β peptide uptake assays *ex-vivo* (**Supplementary Fig. 9**).

In summary, we propose that myelin breakdown contributes significantly to the wear and tear on microglia in the aging brain. Why does myelin overload induce lysosomal inclusions in microglia with time? Myelin is not only an abundant, but also a tightly packed, lipid-rich, and therefore not easy to digest, membrane. We propose that the degradative pathway of microglia represents an Achilles' heel of microglia that is sensitive to over-loading. It is therefore possible that microglia develop lysosomal inclusions as a consequence of the increasing burden of myelin degradation (and possibly also oligodendrocyte turnover⁷), which may contribute to microglia senescence and immune dysfunction in the normal aged brain.

References

1. Nave, K. A. & Werner, H. B. *Annu Rev Cell Dev Biol* **30**, 503-33 (2014).
2. Toyama, B. H. et al. *Cell* **154**, 971-82 (2013).
3. Yeung, M. S. et al. *Cell* **159**, 766-74 (2014).
4. Hildebrand, C., Remahl, S., Persson, H. & Bjartmar, C. Myelinated nerve fibres in the CNS. *Prog Neurobiol* **40**, 319-84 (1993).
5. Peters, A. *J Neurocytol* **31**, 581-93 (2002).
6. Bartzokis, G. *Neurobiol Aging* **25**, 5-18; author reply 49-62 (2004).
7. Young, K. M. et al. *Neuron* **77**, 873-85 (2013).
8. Hanisch, U. K. & Kettenmann, H. *Nat Neurosci* **10**, 1387-94 (2007).
9. Aguzzi, A., Barres, B. A. & Bennett, M. L. *Science* **339**, 156-61 (2013).
10. Prinz, M., Priller, J., Sisodia, S. S. & Ransohoff, R. M. *Nat Neurosci* **14**, 1227-35.
11. Mouton, P. R. et al. *Brain Res* **956**, 30-5 (2002).
12. Poliani, P. L. et al. *J Clin Invest* **125**, 2161-70 (2016).
13. Hoyos, H. C. et al. *Neurobiol Dis* **62**, 441-55 (2014).
14. Streit, W. J., Xue, Q. S., Tischer, J. & Bechmann, I. *Acta Neuropathol Commun* **2**, 142 (2014).
15. Sierra, A., Gottfried-Blackmore, A. C., McEwen, B. S. & Bulloch, K. *Glia* **55**, 412-24 (2007).
16. Yona, S. et al. *Immunity* **38**, 79-91 (2013).
17. Goldmann, T. et al. *Nat Neurosci* **16**, 1618-26 (2013).
18. Grabert, K. et al. *Nat Neurosci* **19**, 504-16 (2016).
19. Hickman, S. E. et al. *Nat Neurosci* **16**, 1896-905 (2013).
20. Readhead, C., Schneider, A., Griffiths, I. & Nave, K. A. *Neuron* **12**, 583-95 (1994).

Figure legends

Figure 1. Microglia clear away myelin fragments in the aging brain. **(a)** High-pressure freezing for electron microscopy was performed on the optic nerve of 6, 12 and 24 month old mice. Arrows point to myelin fragments. **(b)** Quantification of number of myelin fragments (n=4 mice per group, mean +/- SD, one-way ANOVA, ***p<0.0001, followed by Bonferroni's post hoc test, 6 vs 24 months, ***P<0.0001, 12 vs 24 months, ***P<0.0001). **(c)** Confocal image shows co-localization of MBP (green) immunoreactive puncta with Iba1-positive microglia (red) with age. Clipped 3D reconstruction of microglia shows MBP inside the cell. Scale bars: 30µm (overview); 2µm (zoom in); 1µm (clipped 3D). Quantification of number of MBP immunoreactive puncta co-localizing with Iba1-positive microglia in the white matter (n=4 mice per group, mean +/- SD, *P= 0.0415, Student's two-tailed *t* test). **(d)** Visualization and quantification of CD68 (green) positive microglia (Iba1, red) in wild-type mice. Scale bar: 15µm. **(e)** Quantification of lysosomal size in microglia of white and grey matter (n=3 mice per group, mean +/- SD, **P=0.0091, **P=0.0044, *P=0.0408 Student's two-tailed *t* test). **(f)** Left, western blot analysis of purified microglia lysates from 1 year old mice shows MBP in the high-molecular weight region; MBP in myelin is shown as a reference in the right lane. Middle, high-molecular weight species of MBP existed in the Sarkosyl-insoluble (SIF) microglia membrane fraction (1 year old mice, 1 out of 5 representative experiments); MBP in myelin is shown as a reference in the right lane. Right, Sarkosyl extraction on purified myelin shows that myelin-associated MBP is Sarkosyl-soluble (Sarkosyl-soluble membrane fraction, SF). **(g)** Co-localization of myelin fragments (FluoroMyelin, green) with lipofuscin (LF, gray) within microglia (red) in a 24 month old mouse. Scale bars: 2µm. Quantification of number of FluoroMyelin immunoreactive puncta and lipofuscin co-localizing with Iba1-positive microglia in the white matter (n=4 mice per group, mean +/- SD, *P= 0.0356, Student's two-tailed *t* test).

Figure 2. Blocking transport within the lysosomal pathway of microglia results in intracellular myelin storage and age-associated inflammation. **(a)** Confocal image shows co-localization of MBP (green) with Iba1-positive microglia (red). Scale bars: 30µm (overview); 2µm (zoom in). Quantification of MBP immunoreactive puncta in microglia of the white matter in 2 to 9 months old control and Rab 7^{ΔMG} mice (n=3 mice per group, mean +/- SD, **P=0.0058, Student's two-tailed *t* test). **(b)** Co-localization of myelin fragments (FluoroMyelin, green) with lipofuscin (LF, gray) within microglia in 12 months old mice

(n=3 mice per group, mean +/- SD, ***P<0.0001, Student's two-tailed *t* test). Scale bar, 2 μ m. (c) Quantification of lipofuscin volume in μm^3 in Rab 7 $^{\Delta\text{MG}}$ mice as compared to control (n=3 mice per group, mean +/- SD, *P=0.0147, *P=0.0141, **P=0.0059, **P=0.0067, Student's two-tailed *t* test). (d) Visualization and quantification of MHC-II-positive microglia in Rab 7 $^{\Delta\text{MG}}$ and control (n=3 mice per group, mean +/- SD, *P= 0.0168, *P=0.0411, Student's two-tailed *t* test.). Scale bar: 50 μ m. (e) Table of the most significantly upregulated pathways in microglia from Rab 7 $^{\Delta\text{MG}}$ as compare to wild-type mice; and of upregulated pathways in microglia from aged (24 months old) as compare to young (10 weeks old) mice. (f) Venn diagram showing overlap between upregulated genes in microglia of Rab 7 $^{\Delta\text{MG}}$ mice and those upregulated in microglia of aged mice (24 months). Pathway analysis of the common 133 upregulated genes.

Figure 3. Demyelination leads to lipofuscin formation in microglia with time. (a) Demyelination was induced by feeding mice cuprizone and recovery was followed according to the timeline. (b) Quantification of lipofuscin volume in microglia 9, 15 and 37 weeks after cuprizone treatment (n=5 mice per group, mean +/- SD, **P= 0.0011, **P=0.0053, ***P< 0.0001, Student's two-tailed *t* test.). (c) Co-localization of myelin fragments (FluoroMyelin, green) with lipofuscin (gray) within microglia 37 weeks after cuprizone treatment (8 month old mice; n=5 mice per group, mean +/- SD, **P=0.0078, Student's two-tailed *t* test). Scale bars: 2 μ m. (d) Quantification of number of MHC-II positive microglia in cuprizone fed mice (9, 15, 23 and 37 weeks after cuprizone treatment as compared to aged-matched untreated mice; n=5 mice per group, mean +/- SD, ***P<0.0001, Student's two-tailed *t* test). (e) Confocal images and quantification of number of MBP immunoreactive puncta (green) co-localizing with Iba1-positive microglia (red) in 10-month-old wild-type and PMD mice (n=3 mice per group, mean +/- SD, one-way ANOVA, **P=0.0017, followed by Bonferroni's post hoc test, 2 vs 7 months, **P<0.01, 2 vs 10 months, *P<0.05) Scale bars: 30 μ m (overview); 5 μ m (zoom in). (f) Quantification of lipofuscin (LF) volume in microglia of 2, 7, 10 month old PMD and wild-type mice (n=3 mice per group, mean +/- SD, **P=0.0032, ***P<0.0001, Student's two-tailed *t* test).

Supplementary Figures

Supplementary Figure 1. Quantification of myelin fragments in the aging brain. **(a)** Electron microscopy on corpus callosum is shown for a 18-month-old wild type mice. Myelin fragments (arrows) were detected in extracellular space (a), attached to axon, (b) and in the cell (c). Myelin fragments were quantified in 7 and 18-month-old mice (n=3 mice per group, mean +/- SD, **P= 0.0050, Student's two-tailed *t* test). Quantification of myelin fragments attached to axons in 6, 12 and 24-month-old wild type mice (n=3 mice per group, mean +/- SD, one-way ANOVA, **P=0.0024, followed by Bonferroni's post hoc test, 6 vs 12 and 24 months, **P<0.01). **(b)** Confocal images and quantification of number of PLP immunoreactive puncta (green) co-localizing with Iba1-positive microglia (red) in 18-month-old wild-type mice (n=3 mice per group, mean +/- SD, ***P< 0.0001, Student's two-tailed *t* test). Analysis of myelin-associated glycoprotein (MAG), which is localized at the inner, adaxonal space, is shown. MAG immunoreactive puncta show no co-localizing with Iba1-positive microglia (red) consistent with our conclusion that myelin fragments pinch off from the outside of the sheaths (n=3 mice per group, mean +/- SD). Scale bar: 2 μ m.

Supplementary Figure 2. Increase in myelin-microglia contact, lysosomal number and size in the white matter of the brain with age. **(a)** The number of Iba1-positive microglia was quantified in the corpus callosum of 2, 9, 18 and 24 months old mice (n=4 mice per group, mean +/- SD, Kruskal-Wallis-Test, *P=0.016, followed by Mann Whitney post-hoc test indicates significant difference in 9 vs 24 months, *P=0.0411, in 18 vs 24 months, *P=0.044). **(b)** Confocal image of microglia (Iba1, red) and myelin sheaths (MBP, green) in the striatum of 18 month old mice showing the contact of microglia with myelin connected to a sheath. Quantification of number of microglia per area in contact with myelin (n=4 mice per group, mean +/- SD, one-way ANOVA, ***P<0.0001, followed by Bonferroni's post hoc test indicates significant difference in 4 vs 18 months, ***P<0.0001). Scale bars: 7 μ m (overview), 2 μ m (Zoom in), 1 μ m (clipped 3D). **(c)** Visualization and quantification of Lamp1 (red) positive microglia (Iba1, green) in wild type mice. Quantification shows % of Lamp1-positive microglia (n=4 mice per group, mean +/- SD, one-way ANOVA, ***P=0.0006). Quantification shows the size of Lamp1-positive lysosomes in microglia in the white and grey matter (n=4 mice per group, mean +/- SD, **P=0.0047, *P= 0.0285, Student's two-tailed *t* test). Scale bars: 20 μ m. **(d)** Galectin3/Mac2 staining of brain section of 24-

month-old wild type mice. Zoom in show corpus callosum (a), anterior commissure (b) and medial septal nucleus (c) Scale bars: 500 μ m (overview); 50 μ m (Zoom in).

Supplementary Figure 3. FACS analysis show no differences in macrophage number in young and old brain. **(a)** The FACS plot shows the distribution of the brain mononuclear-phagocyte populations stained for CD11b (Y-Axis) and CD45 (X-Axis) in both 8 weeks old and 22 months old animals. Relative percentage over the total viable cells is reported for CNS-associated macrophages (CD11b⁺/CD45^{high}, square). **(b)** Left, The scatter dot-plot shows the percentage of microglia and CNS-associated macrophages in both 8 weeks old and 22 months old animals. No significant difference was observed in microglia and in macrophages number between the two cohorts of animals. (n=7 animals per group, representation of mean value + SEM. Microglia in 8 weeks and 22 months: P=0.1136, Macrophage in 8 weeks vs 22 months: P=0.2037, Student's two-tailed *t* test). Right, the scatter dot-plot shows the percentage of splenic macrophages in both 8 weeks old and 22 months old animals. No significant difference has been observed between the two cohorts of animals (n=5 animals per group, representation of mean value + SEM (splenic macrophage in 8 weeks vs 22 months: P=0,1756, Student's two-tailed *t* test).

Supplementary Figure 4. Number and volume of lipofuscin increases in microglia with age **(a)** Confocal images showing lipofuscin (grey) and microglia (Iba1, red) in a 18 month old wild type mouse. Scale bar: 20 μ m. **(b)** Quantification of lipofuscin volume in μ m³ in 2, 9 and 24 month old mice (n=4 mice per group, mean +/- SD, one-way ANOVA, ***P<0.0001, followed by Bonferroni's post hoc test indicates significant difference in 9 vs 24 months, ***P<0.0001). **(c)** Comparison of lipofuscin volume in μ m³ in the grey and white matter of 18 and 24 month old mice (n=4 mice per group, mean +/- SD, **P=0.01, **P=0.0027, Student's two-tailed *t* test).

Supplementary Figure 5. Myelin uptake results in rapid formation of lipofuscin in microglia **(a)** Confocal image of microglia (Iba1, green) with internalized myelin particles (labeled with PKH26, red), which are associated with lipofuscin (grey) in OHSCs 3 days after adding purified myelin membrane. The clipped 3D reconstruction of internalized myelin shows that myelin is partially connected to lipofuscin. **(b)** Quantification shows percentage of microglia with lipofuscin inclusions in organotypic hippocampal slice cultures (OHSC) 3 days after myelin uptake (n=8-10 slices, mean +/- SD, **P=0.0073, Student's two-tailed *t* test). **(c)** The Pie chart shows the distribution of lipofuscin (LF) and myelin in microglia. **(d)** Visualization

and quantification of lipofuscin volume in microglia within the corpus callosum of *shiverer* mice at P25 (n=3 mice per group, mean +/- SD, *P= 0.0133; Student's two-tailed *t* test). Scale bar: 30µm.

Supplementary Figure 6. Characterization of conditional Rab7 Knockout mice. (a) Strategy for conditional targeting of Rab7 in mice. (b) Timeline diagram for histological analysis of conditional Rab7 knockout mice. (c) Confocal image of cortex of CX3CR1^{+/-CreERT2}:Rab7^{flox/+}:tdTomato+ mice is shown. Microglia were visualized with Iba1 in green and the number of Iba1+/tdTomato+ (red) cells were counted one week after tamoxifen injections (for 5 days with 75mg/kg body weight). tdTomato is expressed in more than 90% of the microglia. Scale bar: 300µm. (d) RT-PCR analysis of Rab7 from isolated microglia from Rab7^{flox/flox} (control) and Rab7^{flox/flox}:CX3CR1^{+/-CreERT2} (Rab 7^{ΔMG}) mice. (e) Confocal image of the cortex of control and Rab 7^{ΔMG} animals 6 weeks after tamoxifen injections is shown. Scale bar: 20µm. Quantification of number of Lamp1-positive microglia per area (n=4 mice per group, mean +/- SD, ***P<0.0001, Student's two-tailed *t* test).

Supplementary Figure 7. Characterization of microglia phenotype in conditional Rab7 knockout mice. (a) Confocal image showing microglia with shorter and less branched processes in Rab 7^{ΔMG} at the age of 10 weeks compared to control mice. Scale bar: 30µm. Quantification of area of microglia processes in µm² in Rab 7^{ΔMG} mice as compared to control (n=3 mice per group, 6 weeks after tamoxifen injection, mean +/- SD, *P=0.0162, Student's two-tailed *t* test). (b) To determine the time-course of FITC-Dextran distribution, we performed injections into the cortex of 10 weeks old wild-type mice and the number of FITC-Dextran-positive microglia was determined at different time points post-injection (n=4-5 mice per time point). No decay of FITC-Dextran signal was seen within 96 hours. (c) FITC-Dextran was injected into the cortex (6 and 18 weeks after tamoxifen injection of P21 mice) of Rab 7^{ΔMG} and control mice and uptake was assessed 7 hours post-injection. Quantification of FITC-Dextran positive microglia (n=3 mice per group, mean +/- SD, *P= 0.0272, Student's two-tailed *t* test). (d) Electron microscopic visualization of myelin fragments (arrows) in corpus callosum of 12 month old Rab 7^{ΔMG} and control mice (48 weeks after tamoxifen injection) in extracellular space (a), in the cell (b) and attached to axon (c). Quantification of number of extracellular myelin fragments (n=3 mice per group, mean +/- SD, *P= 0.0452, *P= 0.0404, Student's two-tailed *t* test).

Supplementary Figure 8. Analysis of transcripts related to the KEGG pathway – cytokine/cytokine receptor interaction. Venn diagram showing overlap between upregulated genes in microglia of Rab 7^{AMG} mice and those upregulated in microglia of aged mice (24 months). Table of upregulated genes.

Supplementary Figure 9. Characterization of the Pelizaeus-Merzbacher mouse model (PMD). (a) Staining of brain sections of 2, 7 and 10 month old PMD mice with antibodies against MBP shows the progressive demyelination. Scale bar: 30µm. (b) Immunohistological analysis of Mac2 and MHC-II in 2, 7 and 10 month old PMD mice. Scale bar: 50µm. (c) FITC-Dextran was injected in to the cortex of 7 month old PMD and wild-type mice. Visualization and quantification of FITC-Dextran positive microglia (n=3 mice per group, mean +/- SD, *P= 0.0465, Student's two-tailed *t* test). Scale bar: 20µm. (d) Microglia-depleted organotypic hippocampal slice cultures (OHSC) were replenished with microglia purified from wild-type or 8-month-old PMD mice. Quantification of 5-carboxyfluorescein (5-FAM)-labelled amyloid-β peptide uptake in OHSCs replenished with microglia (Iba, red) from wild-type or 8-month-old PMD mice (n=4 mice per group, 9-11 slices per mouse, mean +/- SD, *P= 0.0156 Student's two-tailed *t* test). Scale bar: 15µm.

Acknowledgements

The work was supported grants from the German Research Foundation (SI 746/9-1; 10-1; 11-1, RO 4076/3-1, FOR-1336, BI 668/5-1, SFB-TRR43, SyNergy Excellence Cluster), an ERC-Consolidator Grant and the Tschira-Stiftung. N.K. is a recipient of a Marie-Curie fellowship from the INSENS/ FP7-PEOPLE-2013 (607616) framework. We thank Klaus Nave for providing PLP transgenic mice and Wiebke Möbius for electron microscopy support, which is financed by an ERC Advanced Investigator Grant (Axoglia).

Online Methods

Generation of mice with microglia restricted Rab7 mutation

Mice carrying a conditional Rab7 allele where the first exon is flanked by loxP sites ($Rab7^{flox/flox}$)²¹ were crossed with mice with a tamoxifen inducible Cre-mediated recombination system (Cre-ERT2) driven by CX3CR1 promoter to generate mice whose macrophages and microglia lacked Rab7 protein. In the latter mouse line the Cre-ERT2 along with a loxP-flanked neomycin resistance cassette replaces CX3CR1 exon 2²². To remove the Neomycin resistance cassette from $CX3CR1^{CreERT2-neo}$ locus by Cre-mediated excision, these mice were crossed to Ella-Cre (E2A Cre, Deleter-Cre) (The Jackson Laboratory, B6.FVB-Tg(EIIa-cre) C5379Lmgd/J, Stock number: 003724). In the obtained chimeric mice ($CX3CR1^{+/CreERT2-neo}; Ella^{+/Cre}$) removal of neo cassette was confirmed with the PCR using following primer pair, 5'-CACGGGGGAGGCAGAGGGTTT-3'; 5'-GCG GAGCACGGGCCACATTTTC-3' which results in amplification of a 500 bp fragment indicative of $CX3CR1^{+/CreERT2}$ locus without the neo cassette, and a 1800 bp product specific for $CX3CR1^{+/CreERT2}$ locus with neo cassette. To remove Ella-Cre locus from the chimeric mice with excised neo cassette, these mice were mated with C57BL/6J wild type mice. PCR reactions were done using two set of primers as follows: sense Ella promoter (P1): 5'-AGATGACGTAGTTTTTCGCGCTT-3'; antisense Cre (P2): 5'-TCCGGTTATTCAACTTGAC-3', and P3: 5'-TATCTTCTATATCTTCAGGCCGC-3'; P4: 5'-GTGAACGAACCTGGTCGAAATCAG-3'. The combination of P1 and P2 amplified a 387 bp product specific for $Ella^{Cre}$ locus, and the mix of P3 and P4 produced a 223 bp fragment for $CX3CR1^{CreERT2}$ locus. To obtain double transgenic mice ($CX3CR1^{+/CreERT2}; Rab7^{flox/flox}$) two sets of breeding were arranged with $CX3CR1^{+/CreERT2}$ and $Rab7^{flox/flox}$ mice. For genotyping the offspring of these breeding sets two distinct PCR reactions using the combination of P3 and P4 and the following primer pair were done: wild type Rab7 allele: 5'-CTCACTCACTCCTAAATGG-3'; Floxed Rab7 allele: 5'-TTAGGCTGTATGTATGTGC-3'. PCR products amplified by the latter primer pair were a 550 bp band specific for wild-type Rab7 and a 580 bp band representing the floxed Rab7 allele (2 Lox: floxed allele without the Neo cassette).

Tamoxifen induction of of Rab7 gene deletion

Conditional deletion of Rab7 in microglia cells of $CX3CR1^{+/CreERT2}; Rab7^{flox/flox}$ mice was induced by tamoxifen injection at 3 weeks of age. Tamoxifen (Sigma T5648) was dissolved in

filter-sterilized corn oil to make solution of 10 mg/ml. The solution was protected from light, and placed on the roller mixer to be dissolved over night at 37°C. It was administrated via intraperitoneal injection once every 24 hours in 5 consecutive days. The injection dose was determined by weight, using approximately 75 mg tamoxifen/kg body weight. For adult mice, a standard dose of 100 µl tamoxifen/corn oil solution was effective to induce Cre recombinase activity. Control mice of the same genotype received corn oil vehicle only.

Efficiency of CX3CR1-CreERT2 recombinase-mediated deletion in microglia

To test the activity of Cre recombinase in microglia, CX3CR1^{+/CreER}; Rab7^{flox/flox} mice were crossed to reporter mice carrying tdTomato gene which is located downstream of a loxP-flanked STOP cassette. The offspring of this breeding, CX3CR1^{+/CreER}; Rab7^{flox/+}; tdTomato⁺, was injected with tamoxifen at 3 weeks of age. To confirm deletion of Rab7 gene mediated by CX3CR1-driven expression of Cre recombinase, one and six weeks after tamoxifen injection, microglia were isolated and Rab7 transcript measured by relative reverse transcriptase quantitative real-time PCR (RT-qPCR) using primers designed with NCBI Primer Blast software, 5'-GGAATCGGACGTCTCTGTTG-3'; 5'-AGTCCCCCAGGATGATGAC-3'. The expression of the target gene was measured in relation to internal levels of GAPDH and 18srRNA as reference genes. The quantitative PCR was performed using SYBR Green PCR Master Mix according to manufacturer's protocols. The relative change in gene expression was analyzed by Δ Ct method, and normalized to the control samples.

Immunohistochemistry

Animals were anesthetized by intraperitoneal injection of 14% chloral hydrate, perfused transcardially with 4% paraformaldehyde (PFA) using a MPII mini peristaltic pump (flow rate: 3ml/min). Brain tissue was post fixed in 4% PFA overnight and cryoprotected in 30% sucrose in 1x PBS until the brain sank (at least one day). The tissue was bound to the specimen block using Tissue-Tek O.C.T, frozen on dry ice and cut in coronal direction using cryostat Leica CM 1900. The sections were collected in cryoprotective solution (25% glycerol and 25% ethylenglycol in PBS). Free floating sections were rinsed with 1x PBS containing 0.2% Tween-20 in 24-well plate. Permeabilization was performed in 0.5% Triton X-100, the incubation time varied from 10 to 30 minutes depending on primary antibody. To block endogenous mouse tissue immunoglobulins Fab fragment goat anti mouse IgG (1:100) (Dianova) was added for 1 hour at room temperature. The sections were washed briefly and incubated in 100% blocking solution (2.5% FCS, 2.5% BSA, 2.5% fish gelatin in PBS) for 1

hour at room temperature. Primary antibodies, diluted in 10% blocking solution, were added and incubated overnight at 4°C. On the following day, after washing the sections 3 times with PBS for 10 minutes, sections were incubated with secondary antibodies, diluted in 10% blocking solution, for 1 hour at room temperature. The sections were washed with PBS followed by distilled H₂O and mounted using fluorescence mounting medium (Dako) over superfrost plus slides.

3,3-diaminobenzidine (DAB) immunohistostaining was performed using VECTASTAIN® ABC Kit standard. Free floating cryosections were transferred to a 24-well plate, washed three times with PBS. Endogenous peroxidase was blocked with 3% H₂O₂, incubated for 20 minutes at 4°C, and washed out with PBS. Then 100% blocking solution (as before) was added to the sections, incubated for 20 minutes at room temperature. The sections were incubated overnight at 4°C with primary antibodies, diluted in 10% blocking solution. Subsequently, the sections were washed with PBS, incubated with biotinylated secondary antibodies for 1 hour at room temperature. After washing, AB solution containing 20 µl reagent A (Avidin DH) and 20 µl reagent B ((Biotinylated Horseradish Peroxidase H) in PBS was added to the sections and incubated for 30 minutes at room temperature. Following three washes, staining was developed using 3,3'-diaminobenzidine (DAB) staining kit (Vectastain, Vector Laboratories). The incubation time was varied depending on the primary antibody. DAB reaction was stopped with distilled water for 5 minutes on the shaker. Then sections were washed with PBS, and placed on super frost plus microscope slides for 2-3 days to dry. The sections were rehydrated in decreasing concentrations of ethanol, and finally in water, stained with hematoxylin for 1 minute, and dehydrated using increasing percentages of alcohol, cleared in xylol (Chemie Vertrieb GmbH) and mounted with DePeX.

To reduce lipofuscin autofluorescence in old brain tissues for immunohistochemistry²³, the sections dipped briefly in distilled water, and treated with 10 mM CuSO₄ (Fisher Scientific; Pittsburgh, PA) in a buffer containing 50 mM ammonium acetate and 100 µM EDTA, pH 4.5 for 90 min on a shaker. The sections were washed briefly in distilled H₂O, and transferred to PBS. Autofluorescence was removed by means of dye separation tool on Leica SP5 confocal microscope.

Antibodies

Primary antibodies: Iba1 (Ionized calcium binding adapter molecule 1, Wako), Mac2 (Galectin 3, Biologend) and MHC-II (major histocompatibility complex class II, eBioscience), Mac3 (BD Pharmingen), CD11b (Complement receptor 3 or Mac1; Bio-Rad), CD16/32 (Fcγ

receptor II/III, BD Pharmingen), CD45 (Bio-Rad), MBP (Myelin Basic Protein, Convance) against myelin, Lamp1 (lysosomal-associated membrane protein 1, Santa Cruz Biotechnology) for lysosomes. Secondary antibodies: For DAB staining we used goat anti rat biotinylated immunoglobulin G (Vector Laboratories) and for fluorescence microscopy Alexa Flour 488, 647, and 555-conjugated antibodies (Invitrogen) were used.

Electron microscopy

For high pressure freezing mice were killed by cervical dislocation, and freshly extracted optic nerves were cryofixed using a high-pressure freezer HPM100 (Leica) and further processed by freeze substitution and EPON-embedding following the “tannic acid-OsO₄ protocol” as described in Möbius et al.²⁴. Cross ultrathin sections (50nm) of the retinal ends were obtained with an Ultracut S ultramicrotome (Leica) and contrasted as described previously²⁵.

For conventional fixed preparations the mouse brain was fixed by transcardial perfusion using 4% paraformaldehyde and 2.5% glutaraldehyde in 0.1M phosphate buffer containing 0.5% NaCl. The brain was extracted, post fixed in the same fixative solution overnight. The tissue was sectioned into 200 µm thick vibrotome sections. Rostral and caudal regions of corpus callosum was cut and post-fixed in a solution of 1% osmium tetroxide in 0.1M phosphate buffer (pH 7.4) for 30 minutes at room temperature. Following washing with distilled water the sections were stained with 0.5% uranyl acetate in 70% ethanol for one hour, dehydrated in a serial dilution of ethanol, and cleared in propylene oxide and embedded in Epon, incubated at 60°C for 24 hours. The tissues in Epon blocks was then trimmed and reoriented so that ultrathin (60 nm) cross section of midline corpus callosum could be cut using ultramicrotome. Ultrathin sections were collected on collodion-coated copper grids.

Image processing and analysis

Images were processed and analyzed with Imaris (64x version 7.7.1) and ImageJ 1.41 image processing software. To estimate the number of Iba1 positive cells, confocal stacks (step size: 0.8µm) were captured in the z-direction from the whole region of interest with 20X or 40X objectives of a Leica TCS SP5 confocal microscope. An area in the size of 1mm² in the region of interest was selected, the total number of Iba1 positive cell bodies and as well as the number of Iba1 positive cells with internalized components (such as FITC-Dextran or MBP or lipofuscin) were counted using cell counter plugin in ImageJ. In addition, to confirm the quantification performed by ImageJ, cell counting was done automatically using Imaris

software. Briefly, a region of interest was segmented and spots layer was created (radius scale: 8) for each marker (Iba1 and FITC/MBP/LF) in the corresponding channel, using those spots the cells were counted automatically. The colocalized spots were defined in the distance of 0.2 μ m (threshold value).

The size of lipofuscin accumulations within at least 40 microglia cells was quantified. Individual cells were analyzed using Imaris software as following. An area the size of 1 mm² in cortical white matter as well as striatum was chosen and confocal z-stacks (step size: 0.8 μ m) were acquired with a Leica TCS SP5 confocal microscope (40x objective). A three dimensional image was generated in Imaris' Surpass view. The "surface" option in tool bar was selected then in the third channel (Far red), a region of interest including lipofuscin compartment within a single cell was segmented. The threshold was manually set in a way to carefully cover the whole volume of compartment in the cell by creating a surface.

To determine myelin and microglia contact area, confocal z-stacks (step size: 0.8 μ m) were taken in striatum with 40X objective of a Leica TCS SP5 confocal microscope. A three dimensional image from the whole area was created using surpass view in Imaris software. To measure the surface area of each microglia cell in contact with myelin a single cell, including cell body and all the processes in total focus, was segmented. By choosing "spots" option in tool bar and adjusting the appropriate threshold the entire cell was covered. Next, the area labeled with MBP against myelin around the cell of interest was segmented. By activating the "surface" in the tool bar a surface was created over that area. Total number of spots (representing cell process or cell body) and also number of close spots to the surface (representing myelin) was calculated using distance threshold 0.4. Finally, using these numbers the percentage of cell area in contact with myelin was calculated. 20 cells were analyzed.

Imaris software was used to measure the area microglia processes. 40 cells taken from random regions of the brain were analyzed. Confocal z-stacks (step size: 0.8 μ m) were acquired from different areas in cortical white matter, corpus callosum and striatum using a Leica TCS SP5 confocal microscope with 40x objective. A three dimensional image was generated in Imaris' Surpass view. Then a microglia cell with the whole cell body and all the processes in focus was segmented as a region of interest. Subsequently, to measure the whole area occupied with the single microglia, a surface was created all over the cell. Additionally, the cell body of each microglia cell was also segmented, and its area was quantified by creating a surface.

Eventually, the area of cell body was subtracted from the whole cell area to obtain the area of microglia processes.

To visualize inside the cell, the surface was cut using the clipping plane in Imaris software.

Microglia isolation

For optimal dissociation of tissue samples, brain tissue from 12-month-old C57Bl/6 wild type mice was dissociated using a Neural Tissue Dissociation Kit (Papain) (Miltenyi Biotec). Briefly, the mice were perfused by cold PBS, the brain was removed and cut into small pieces then the tissue was dissociated by enzymatic digestion. Next, the tissue was dissociated mechanically by wide and narrow-tipped pipettes until no tissue pieces remained. The suspension was applied to a 40 µm cell strainer, and washed twice with Hank's balanced salt solution (HBSS). To remove myelin, the tissue pellet was resuspended in 37% Percoll (Sigma) and overlaid on 70% Percoll in DMEM containing 2% FCS (Fetal Calf Serum), centrifuged at 500g for 30 minutes. A membrane fraction, which formed on the top of the 37% Percoll gradient, was removed using vacuum pump. The thin fraction, containing single cell suspension, in the interface between 37% and 70% percoll was then carefully taken out and washed with the medium and MACS rinsing solution (0.5% BSA and 2mM EDTA in PBS). Microglia were then isolated from the single-cell suspension by MACS® Technology. The suspension was incubated with CD11b (Microglia) MicroBeads (Miltenyi Biotec) at 4°C for 15 minutes, after washing with MACS rinsing solution, the pellet was resuspended in 500 µl of the same buffer, applied on a MACS column placed in the magnetic field, following three times wash with 500 µl MACS buffer, CD11b positive cells (microglia) were then flushed out of the column, centrifuged at 400 x g for 8 minutes at 4°C. The pellet was resuspended in 1 ml PBS and washed one more time. The final pellet was flash frozen in liquid nitrogen, and stored at -80°C for future use.

Preparation of Sarkosyl-insoluble membrane fractions

The preparation of Sarkosyl-insoluble membrane fraction was performed as described previously ²⁶. Briefly, the pellet containing 1.5×10^6 microglia isolated from 12-month-old mice was resuspended in PBS was resuspended in 300µl 10% Sarkosyl and 1 µl of 10 µg/ml β-mercaptoethanol and incubated at 4°C for 4 hours on a roller. To prepare the Sarkosyl-insoluble fraction, the solution was transferred in Beckman 1.5 ml tubes, and centrifuged at 130000 x g for 35 min at 4°C. The pellet was resuspended in 1ml cold TBS (50mM Tris pH 7.6, 150mM NaCl) and, centrifuged again at 130,000 x g for 35 min at 4°C. The resulting pellet was washed one more time in cold TBS. The supernatant was removed carefully and the final pellet (Sarkosyl-insoluble fraction, SIF) was flash frozen and stored at -80°C for

further use. To examine the solubility of myelin membrane in Sarkosyl, the same experiment was done with 1.5 µg pure myelin membrane. Western blotting was performed using a polyclonal MBP antibody (Dako, 1:1000).

Myelin isolation and purification

The myelin from 8-week-old C57BL/6 mouse brains was isolated by sequential centrifugation on discontinuous sucrose gradient according to a protocol previously described²⁷ with some modifications. The ultracentrifugation was done using a SW41 Ti rotor. The brain tissues were homogenized with a Dounce homogenizer in a solution containing 10 mM HEPES, 5 mM EDTA, 0.3 M sucrose, and protease inhibitor. The homogenized tissue was layered on a sucrose gradient composed of 0.32 M and 0.85 M sucrose prepared in 10 mM HEPES, 5 mM EDTA. (pH 7.4), centrifuged at 75,000g for 30 minutes with low deceleration and acceleration. The crude myelin fraction was removed from the interface, suspended in distilled water, and centrifuged at 75,000g for 15 minutes. The pellet was subjected to two rounds of hypo-osmotic shock by resuspension in 10 ml ice-cold water, centrifuged at 12,000g for 10 minutes. For purification of myelin, the pellet obtained from the last step was dissolved in HEPES/EDTA buffer, and placed over the sucrose gradient; all the centrifugation steps and hypo-osmotic shocks were repeated as before. Eventually, the purified myelin pellet was resuspended in 1 ml HEPES/EDTA buffer and stored at -20°C.

Organotypic hippocampal slice cultures

Organotypic hippocampal slice cultures (OHSC) were prepared from P0-P2 C57BL/6N mice according to a slightly modified protocol²⁸. OHSCs were kept in a humidified atmosphere at 35°C and 5% CO₂. Medium was changed every other day.

To deplete microglia, OHSC were treated with clodronate disodium-salt. Clodronate was solved in ultra-pure H₂O in a concentration of 1 mg/ml. OHSC were incubated with 100 µg clodronate per ml standard culture medium for 24 hours at 35 °C. Subsequently, OHSC were rinsed with warm PBS and placed on fresh culture medium. Microglia-depleted OHSC were kept at least for 7 days *in vitro* before experiment. Medium was changed every other day.

To replenish microglia, microglia were isolated from 8-month-old wild type and PMD mice based on density gradient centrifugation using Percoll (Sigma). Mice were perfused with cold 1x PBS, and only cerebrum was homogenized in a HBSS containing 0.5% glucose (Sigma) and 15mM HEPES using a Dounce homogenizer. The tissue was dissociated mechanically by wide and narrow-tipped pipettes until no tissue pieces remained. The suspension was applied

to a 40µm cell strainer, and washed twice with HBSS. Subsequently, the tissue pellet was resuspended in 75% Percoll (Sigma) and overlaid on 25% Percoll in PBS, centrifuged at 800g for 30 minutes. A cloudy layer, containing microglia, in the interface between 25% and 75% percoll was then carefully collected and cell pellet was obtained by centrifugation at 200g for 10 minutes. The cell number was adjusted to obtain a number of 1000 cell/µl. Subsequently, 2µl of cell suspension (2000 cells) were added on top of each microglia-depleted tissue slice. The replenished OHSCs were maintained for 2 weeks so that the newly added microglia were distributed evenly and ramified²⁸.

To perform uptake experiments, 5-carboxyfluorescein (5-FAM)-labeled synthetic human amyloid β (Aβ) peptide with amino acids 1–42 was purchased from AnaSpec, and prepared according to the instruction described previously²⁹. Before adding on OHSCs, Aβ was sonicated for 10min in an ultrasound water bath and then mixed by vortex for 2 min. The replenished OHSCs were treated twice with Aβ containing solution (each time 2µl of a 15µM solution) every second day. 24 hours after the last treatment OHSCs were analyzed.

Purified myelin pellet was resuspended in sterile PBS and protein concentration in myelin was then measured by Bio-Rad Protein Assay, based on the method of Bradford. For immunofluorescence analysis, myelin was labeled with PKH26 (Sigma), and then washed in PBS by centrifugation at 15000g. The final pellet was resuspended in culture medium. Before adding to the slice culture, myelin was sonicated for 10min in an ultrasound water bath.

To perform myelin uptake experiments, 4µg purified myelin was added twice onto each slice twice. The first treatment started, 3 days after OHSC culture and the second one day later. OHSCs were fixed with 4% PFA 3 days after the last treatment with myelin. Medium was changed every second day.

In vivo endocytosis assay

Mice were anesthetized intraperitoneally with a solution (0.15 ml/25 g) containing 4% Rompun™ 2% (xylazine) (Bayer DVM for veterinary professionals) and 12.5% ketamine 10% (Medistar) in 0.9% NaCl, placed into stereotaxic apparatus (Kopf Instruments), and 1.5 µg FITC-conjugated Dextran (40 kDa; Molecular probes, Eugene, OR, USA) in sterile PBS was injected by a glass capillary microinjector at the following coordinates relative to bregma: 0.3mm anterior, 1.2 mm lateral and 1.2 mm below cortical surface. 7 hours after injection the mice were perfused and the brain tissues were prepared and stained as described above.

Cuprizone treatment

Six weeks after tamoxifen injection, Rab7 conditional knockout mice as well as corresponding control mice were treated with 0.2% cuprizone for four weeks. The animals were returned to normal diet for another four weeks to induce remyelination. Animals were continued on normal diet for 5, 11, 19 or 33 weeks after completed remyelination (recovery). Age-matched controls received normal diet without cuprizone throughout the whole experiment.

Flow cytometry

8 weeks old and 22 months old mice (7 per group) were anesthetized with ketamine hydrochloride (Ketavet, Pfizer; 100 mg/kg body weight) and xylazine (Rompun, Bayer HealthCare; 20 mg/kg body weight) and transcardially perfused with ice-cold PBS. All following steps were carried out on ice and using ice-cold solutions. Microglia isolation was carried out as previously described²⁸. Briefly, perfused brains have been carefully removed and placed into a petri dish and finely shredded with a scalpel. Subsequently, brain tissue were transferred into a tissue masher tube and slowly homogenized. Brain homogenate was eventually flushed with a Pasteur pipette through a 70µm strainer filter and rinsed with 50ml of Gibco HBSS 1X media (Life Technologies). Cellular fraction was collected into a 50ml falcon tube and pelleted by centrifugation. Supernatant was discarded and pellet was resuspended in 35% Percoll gradient (GE healthcare). The myelin fraction was removed by centrifugation on a density gradient made as follow: 35% Percoll (bottom part) and PBS (upper part). Centrifugation was carried out at 1000g for 30 minutes at 4°C (without break). After centrifugation myelin fraction was settled at the interface between the two gradients, while the cellular fraction was collected in the pellet. Pellet was resuspended in PBS, centrifuged (pellet wash) and eventually transferred into FACS tubes.

Splenocytes were collected by squeezing fragmented spleen tissue on a 70µm strainer filter, subsequently rinsed with 50ml of PBS. Cellular fraction was collected into a 50ml falcon tube and centrifuged. Pellet was eventually transferred into FACS tubes.

Brain pellets devoid of myelin, as well as spleen pellets, were treated as follows: 15 minutes incubation with FC-receptors blocker (1:100), followed by 30 minutes incubation with anti-mouse CD45-FITC and anti-mouse CD11b-APC (1:200). Between each step pellets were washed in PBS and centrifuged at 1000g per 5 minutes at 4°C. All staining products are provided by eBioscience. Immediately before reading, samples were incubated with DAPI (1:1000) for 1 minute. DAPI is poorly permeable through the cell membrane therefore its signal has been used to identify and select viable cells.

FACS analysis was performed with 8-color LSR Fortessa from Becton Dickinson (BD Bioscience). Cells were hierarchically gated as follows: 1) FSC/SSC (selection microglia population depending on cell granularity and dimension); 2) FSC-A/FSC-H selection single cells); 3) FSC-A/DAPI (selection viable cells); 4) final gating on microglia (CD11b+/CD45^{int}) and brain macrophages (CD11b+/CD45^{hi}). CD45-FITC fluorescence intensity higher the 10⁴ were arbitrary addressed as “CD45^{hi}”. In spleen samples CD11b+/CD45^{hi} population were addressed as “splenic macrophages”, while the CD11b-/CD45^{hi} population labeled as “splenic”.

RNA Sequencing

The sorted cells were homogenized in RLT buffer using QIAshredder (QIAGEN) and the total RNA was extracted using micro-RNAeasy Kit (QIAGEN) and cDNA was synthesized using Ovation RNA-Seq System V2 (NuGEN). 1 µg of cDNA was used as input for Ion Xpress™ Plus Fragment Library Kit (ThermoFisher Scientific) to generate barcoded libraries. Barcoded libraries were then quantified using qRT-PCR (KAPA Library Quantification Kit). Barcoded libraries were then pooled and clonally amplified on Ion Spheres (Ion One Touch 200 Template Kit v2, ThermoFisher Scientific) and were sequenced on an Ion Proton sequencer (ThermoFisher Scientific).

Data analysis

Raw reads were sorted based on barcodes and were subjected to quality analysis using FASTQC. The sequences were subsequently aligned to the genome of *Mus musculus* (GRCm38/Mm10) using the TMAP aligner with default parameters. The reads mapping to unique locations were quantified using RefSeq Gene Annotations(v73) into genes. Differential gene expression analysis and hypergeometric pathway analysis using KEGG genesets was performed using a commercial platform (Partek). Genes with fold change greater than 2 and p-values less than 0.05 were considered for further hypergeometric pathway enrichment analysis.

Ethics Statement

All experiments were approved and conducted in accordance with animal protection laws approved by the Government of Lower Saxony, Germany. C57BL/6 mice were used for all experiments. They were kept in groups of three in standard plastic cages and maintained in a

temperature-controlled environment ($21 \pm 2^\circ\text{C}$) on a 12-h light/dark cycle with food and water available ad libitum.

Statistics

Statistical analysis was done using GraphPad Prism (GraphPad Software, Inc.) and SPSS software. To compare two groups, a two-tailed Student's *t*-test was applied. One-way analysis of variance (ANOVA) followed by Bonferroni posttest post-hoc test was performed for comparison of more than two groups. When the sample size was small, non-parametrical test such as Kruskal-Wallis test followed by Mann-Whitney test was applied. To analyze the interaction of age and genotype, or age and brain region, two-way ANOVA followed by Bonferroni posttest was used. A *p* value of <0.05 was considered significant in all tests. All values are represented as mean \pm SD.

21. Roy, S. G., Stevens, M. W., So, L. & Edinger, A. L. *Autophagy* **9**, 1009-23 (2013).
22. Jung, S. et al. *Mol Cell Biol* **20**, 4106-14 (2000).
23. Schnell, S. A., Staines, W. A. & Wessendorf, M. W. *J Histochem Cytochem* **47**, 719-30 (1999).
24. Mobius, W. et al. *Methods Cell Biol* **96**, 475-512 (2010).
25. Snaidero, N. et al. *Cell* **156**, 277-90 (2014).
26. Nukina, N. & Ihara, Y. *J Biochem* **98**, 1715-8 (1985).
27. Larocca, J. N. & Norton, W. T. *Curr Protoc Cell Biol* **Chapter 3**, Unit3 25 (2007).
28. Masuch, A., Shieh, C. H., van Rooijen, N., van Calker, D. & Biber, K. *Glia* **64**, 76-89 (2016).
29. Hellwig, S. et al. *Sci Rep* **5**, 14624 (2015).

Figure-1

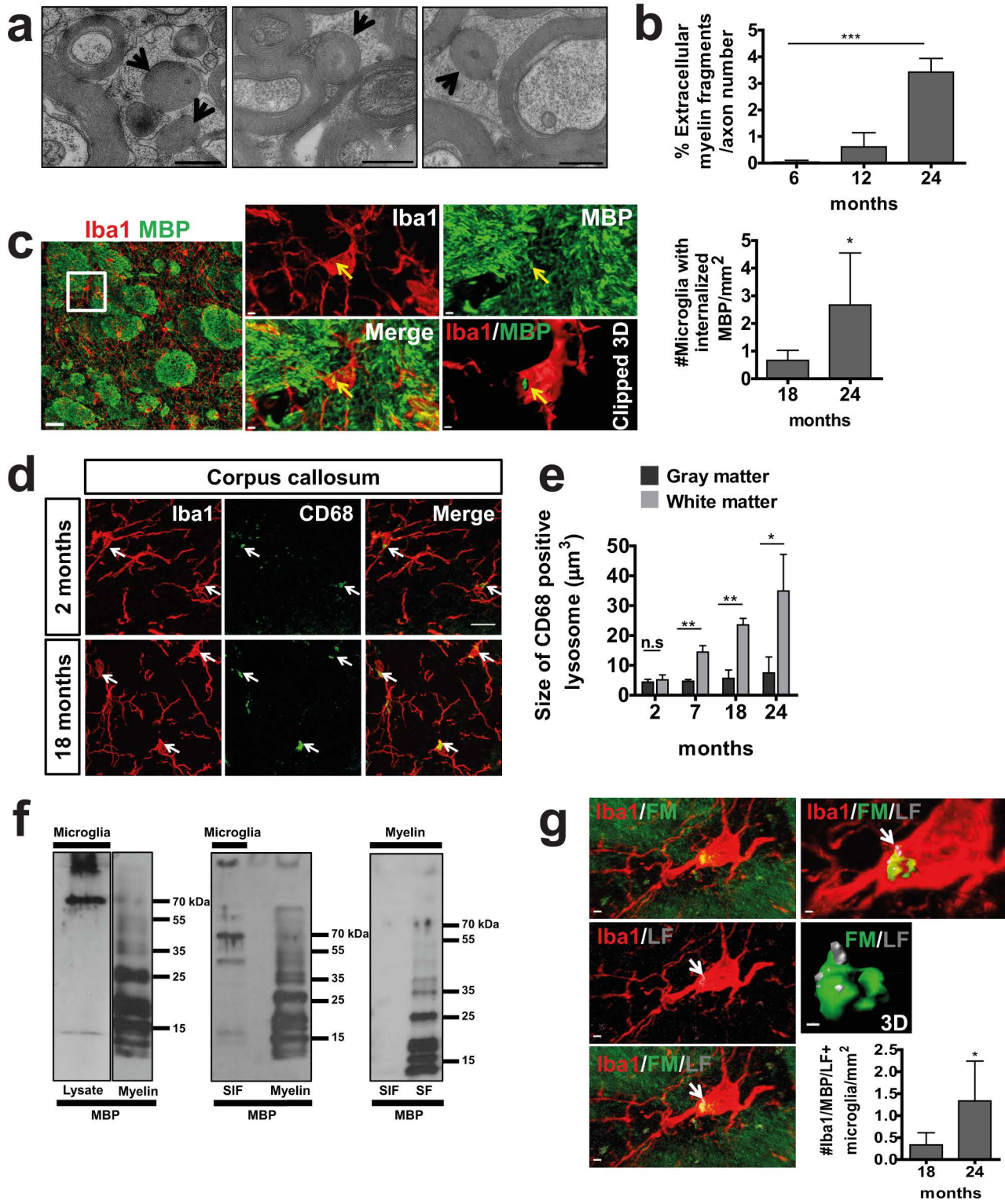
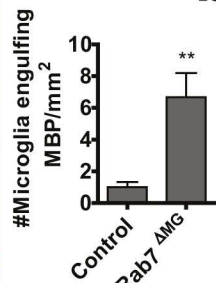
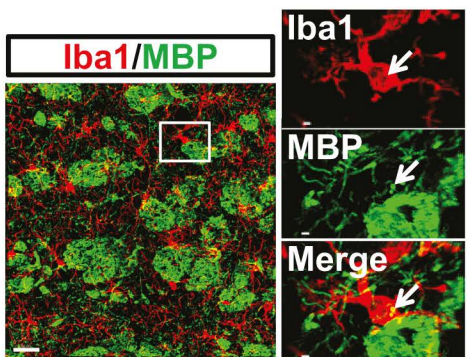
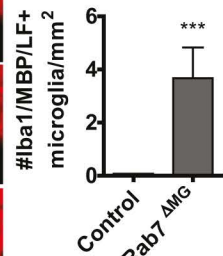
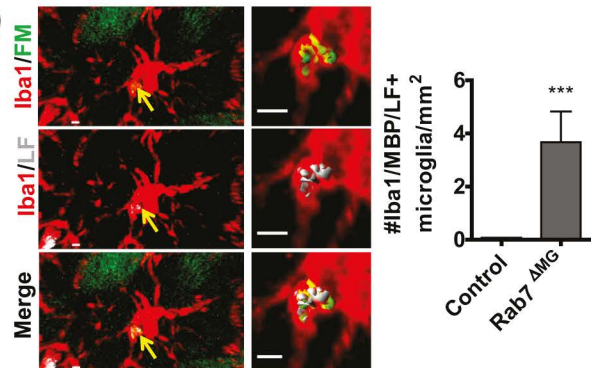


Figure-2

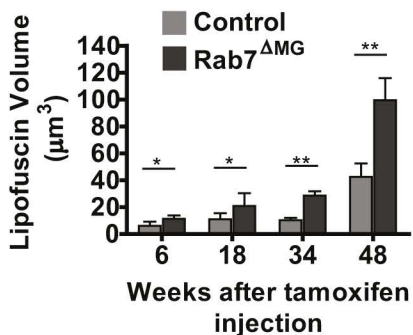
a



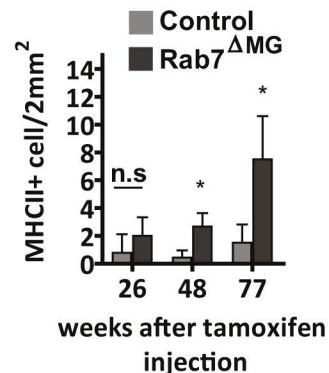
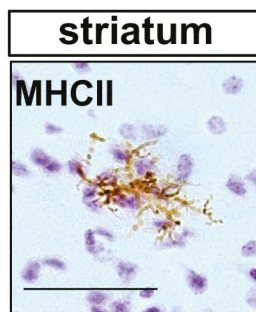
b



c



d



e

KEGG Pathway	P value (Rab7 ^{ΔMG} vs Control)
1 CYTOKINE_CYTOKINE_RECEPTOR_INTERACTION	2,88E-07
2 CHEMOKINE_SIGNALING_PATHWAY	3,32E-04
3 CELL_ADHESION_MOLECULES_CAMS	1,35E-03
4 ENDOCYTOSIS	2,43E-03
5 ECM_RECEPTOR_INTERACTION	8,96E-03
6 NOD_LIKE_RECEPTOR_SIGNALING_PATHWAY	1,18E-02

KEGG Pathway	P value (Wt aged vs young)
1 CYTOKINE_CYTOKINE_RECEPTOR_INTERACTION	0,0010179
2 P53_SIGNALING_PATHWAY	0,00523481
3 CELL_CYCLE	0,00719541
4 CELL_ADHESION_MOLECULES_CAMS	0,00762406
5 NOD_LIKE_RECEPTOR_SIGNALING_PATHWAY	0,00942117

f

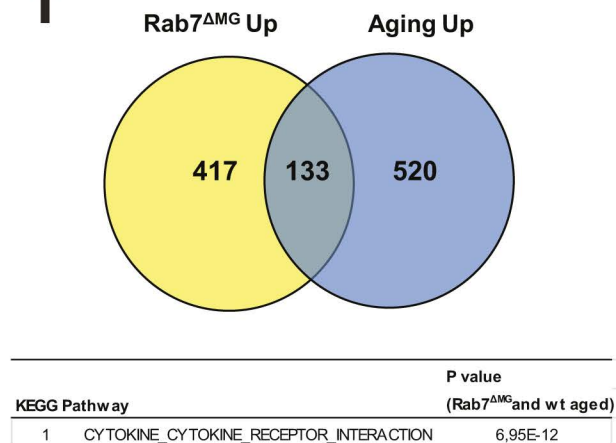


Figure-3

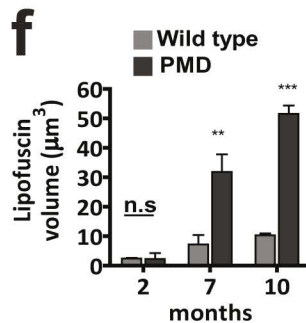
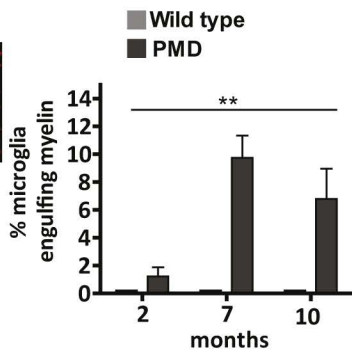
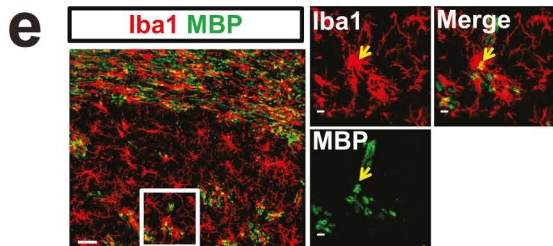
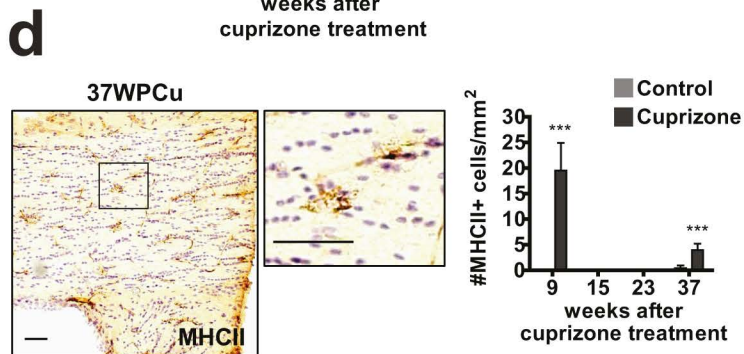
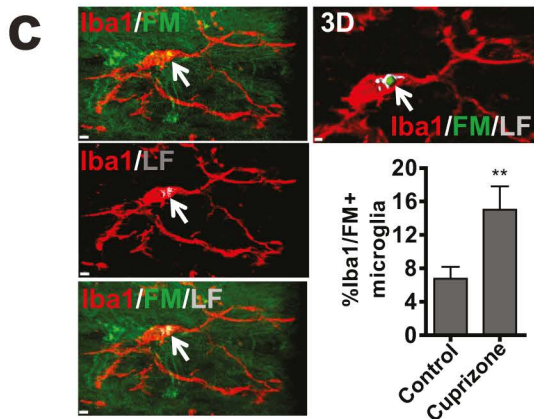
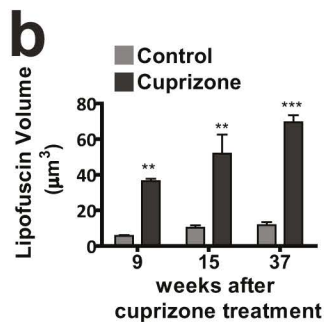
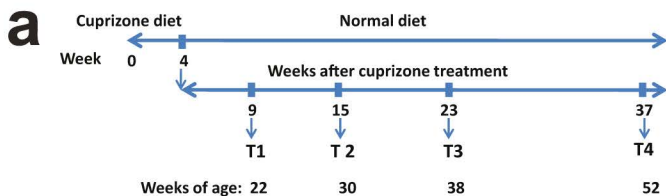
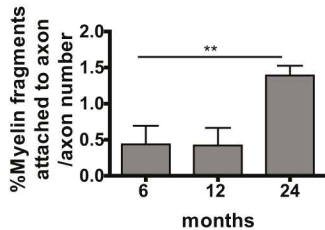
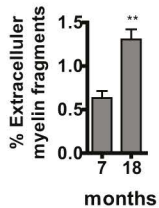
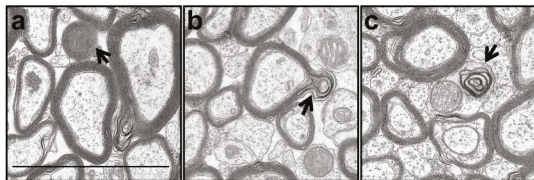


Figure S1

a



b

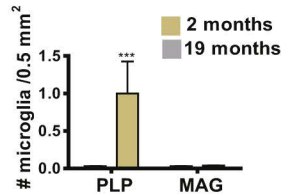
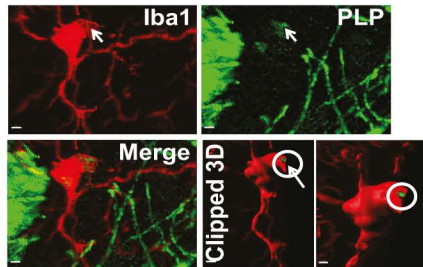


Figure S2

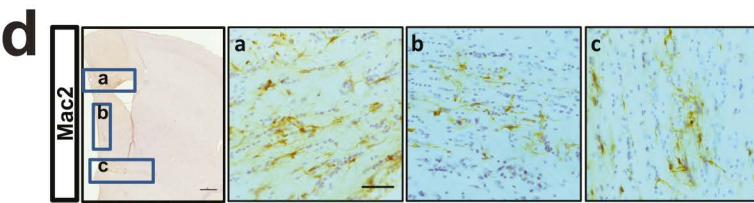
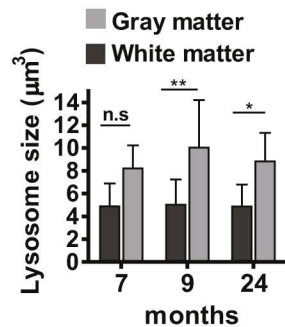
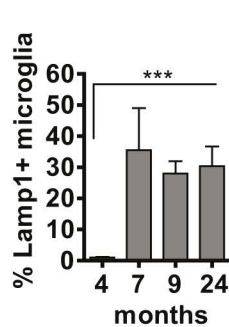
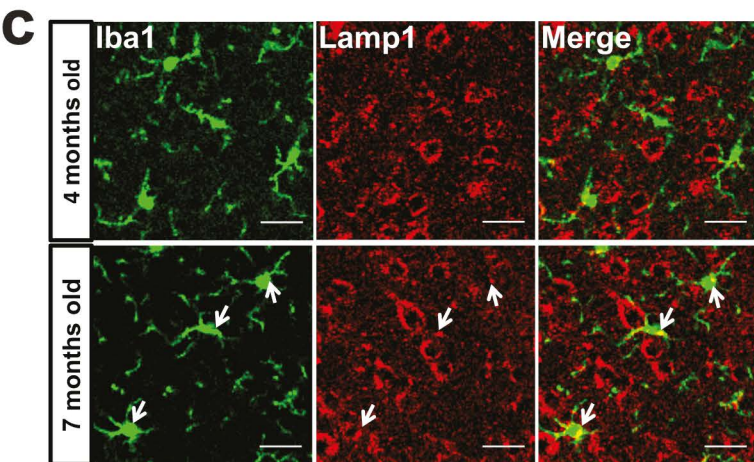
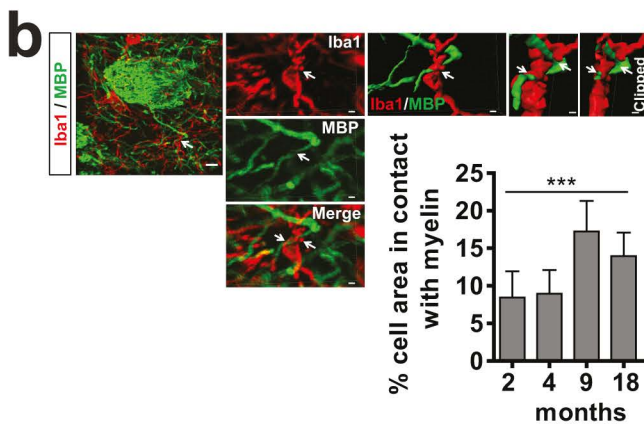
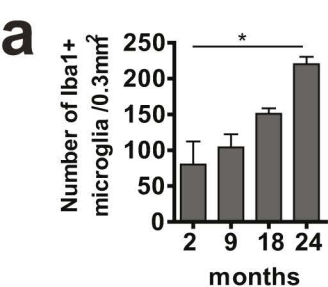
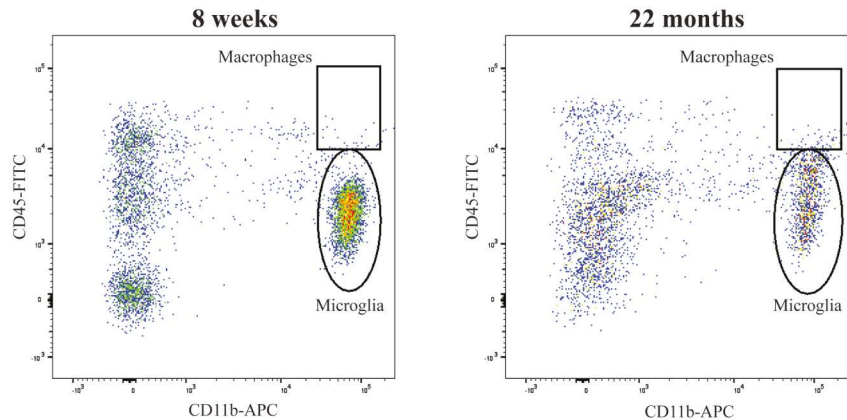


Figure S3

a



b

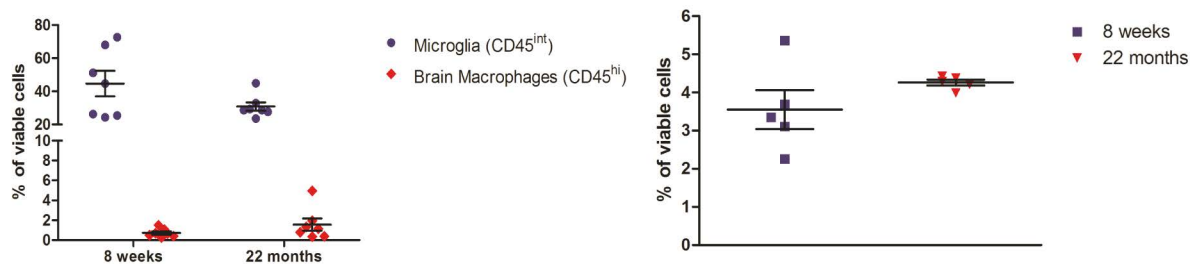
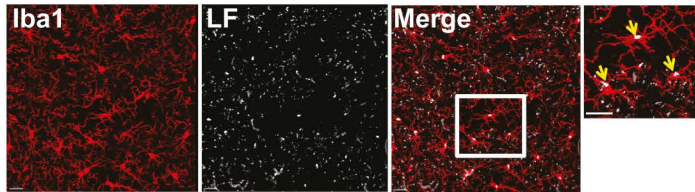
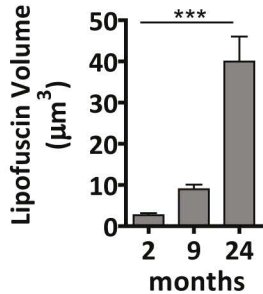


Figure S4

a



b



c

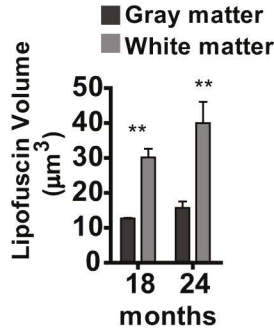


Figure S5

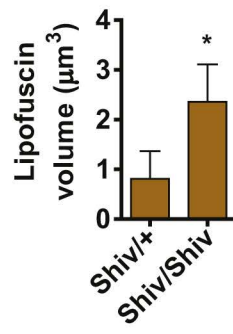
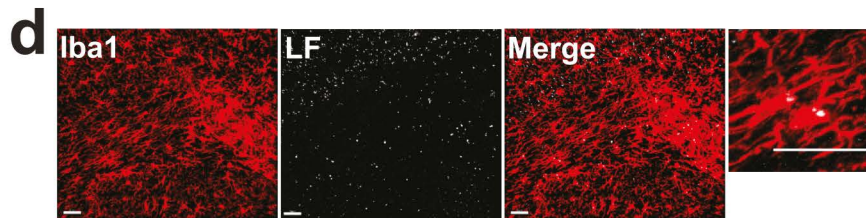
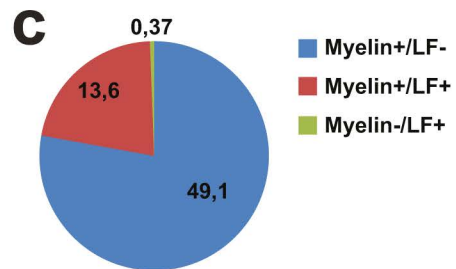
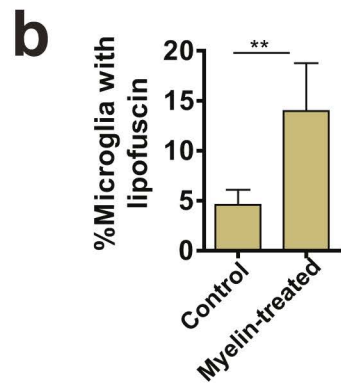
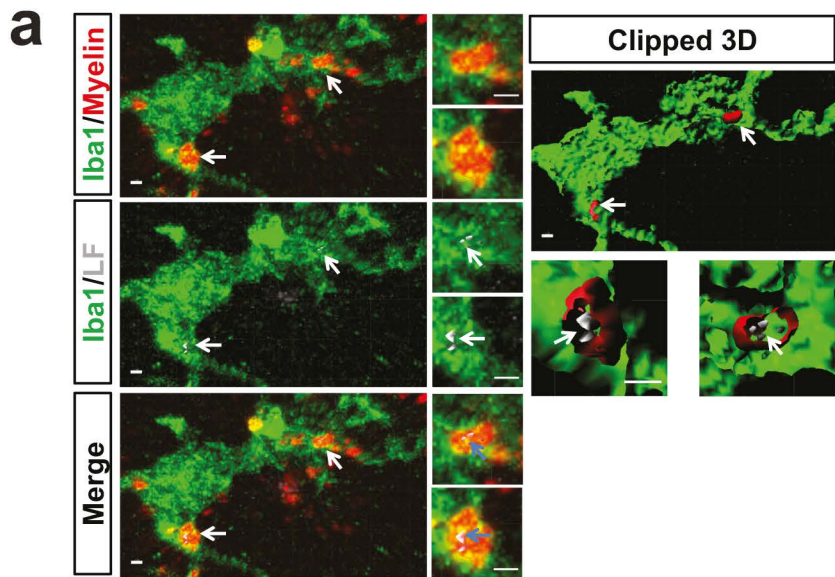
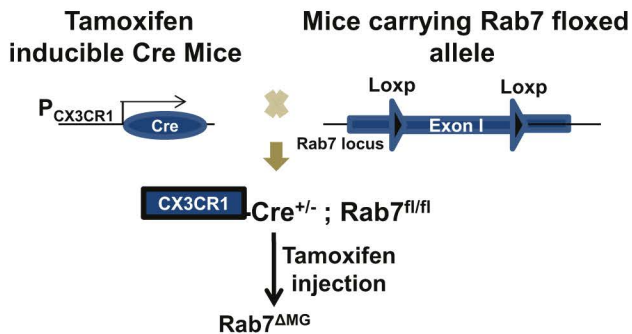
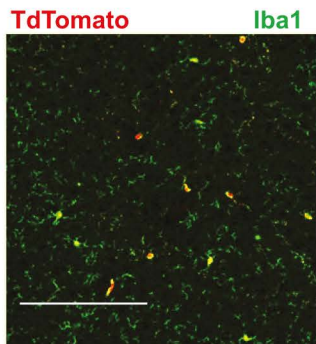


Figure S6

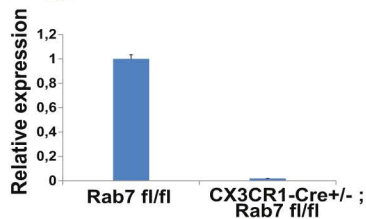
a



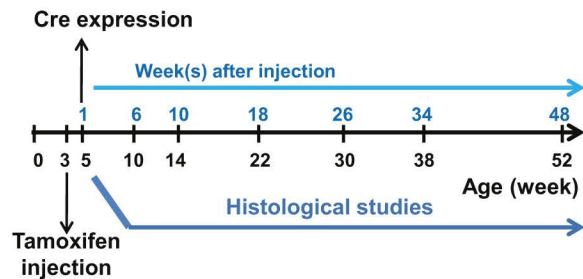
c



d



b



e

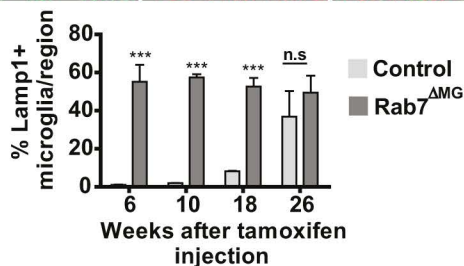
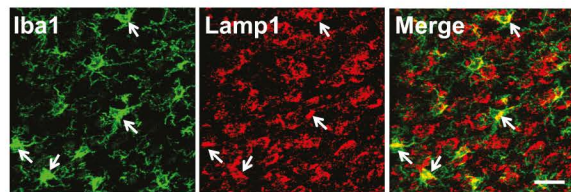


Figure S7

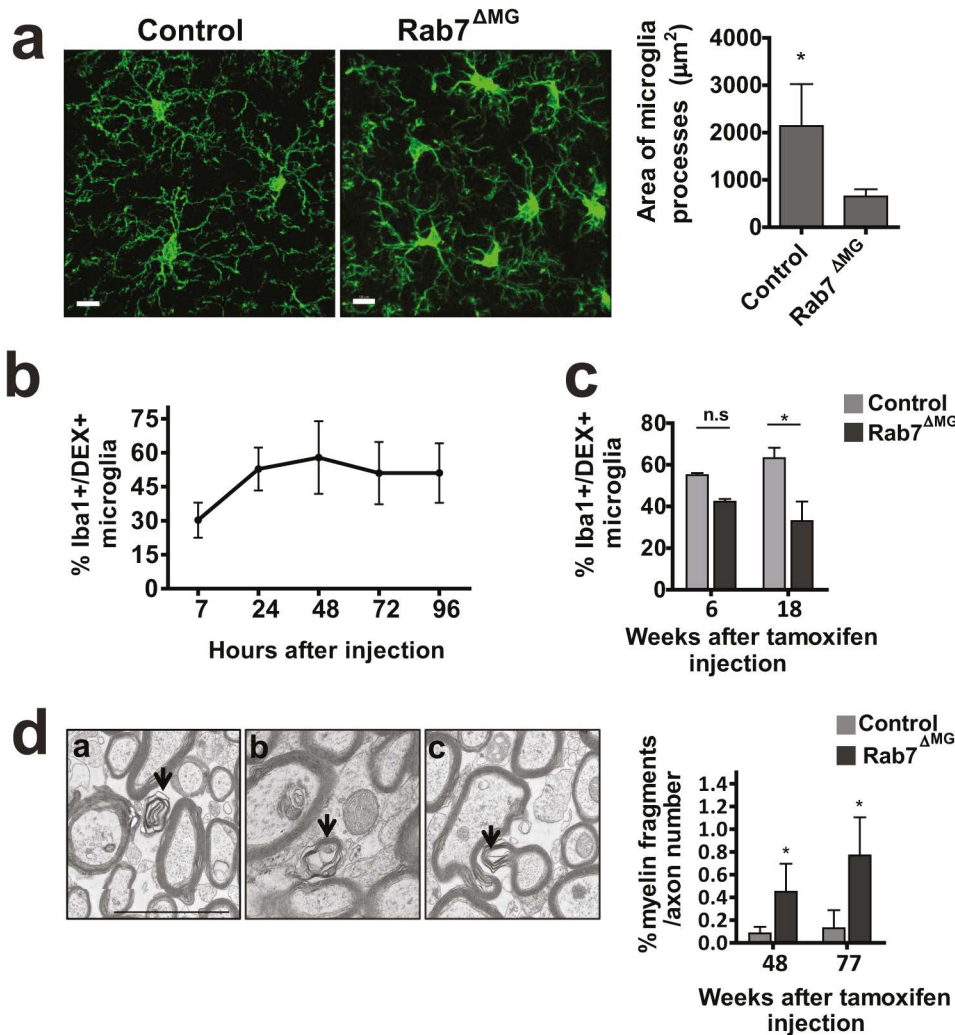
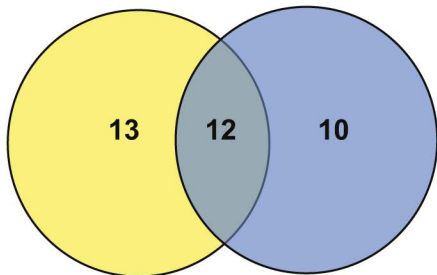


Figure S8

Rab7^{ΔMG} Up

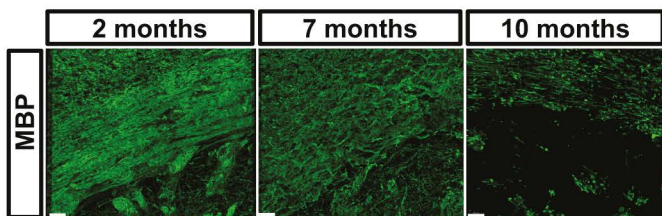
Aging Up



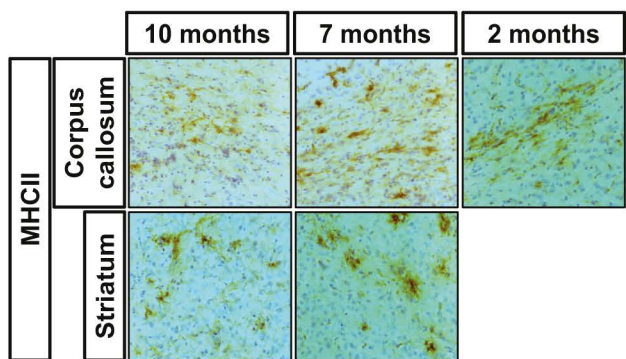
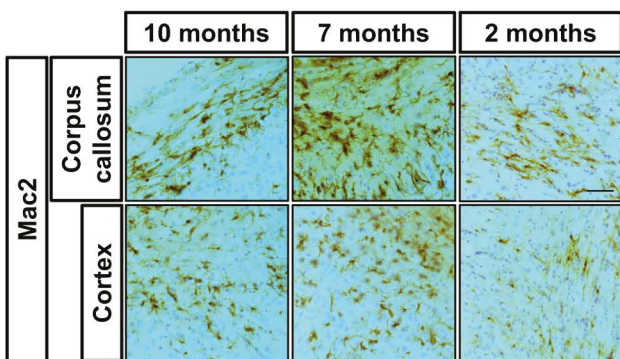
Rab 7 KO Up	Aging Up	Common in both
CCL2	TNFSF8	IL17RB
IL17RB	IL17RB	CCR2
CCL22	CCL7	CXCR4
PRLR	CCR2	IL1R2
CCL24	CXCL10	OSM
CCR2	CXCR4	LTB
CXCR4	IL1R2	CXCR2
IL1R2	OSM	CXCR1
KIT	CXCL13	IFNB1
OSM	LTB	IL1B
LTB	CXCL9	CXCL2
GHR	TNFSF13B	BMP7
IL18RAP	TNF	
IL18R1	CXCR2	
CX3CR1	CXCR1	
CXCL1	IL2RG	
CXCR2	IFNB1	
CXCR1	TNFRSF10B	
TNFRSF18	IL1RAP	
IL2RB	IL1B	
CCR1	CXCL2	
IFNB1	BMP7	
IL1B		
CXCL2		
BMP7		

Figure S9

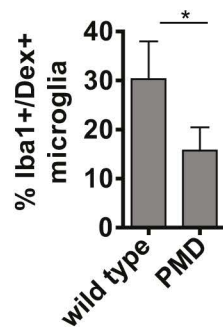
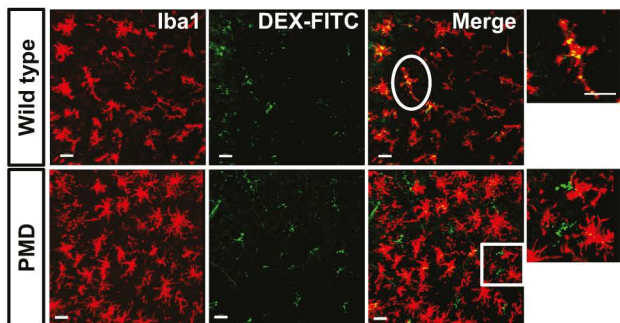
a



b



c



d

